Chapter 3

Insight into the physico-chemical properties of a subducted slab from garnet zonation patterns (Sesia Zone, Western Alps)

MATTHIAS KONRAD-SCHMOLKE, JOCHEN BABIST, MARK R. HANDY

Freie Universität Berlin, Department of Geosciences, Malteserstr. 74-100 12249, Berlin

and

PATRICK J. O´BRIEN

University of Potsdam, Dept. of Geosciences, Karl-Liebknecht-Strasse 24-25, 14476 Golm

3.1 ABSTRACT

Garnets in continentally-derived high-pressure (HP) rocks of the Sesia Zone (Western Alps) have three different chemical zonation patterns, depending on sample locality. Comparison of observed garnet zonation patterns with thermodynamically modelled patterns shows that the different zonation patterns are caused by differences in the water content of the subducted rocks during prograde metamorphism. Zonation patterns of garnets from water-saturated host rocks show typical prograde chemical zonations with steadily increasing pyrope content and increasing XMg, together with bell-shaped spessartine patterns. In contrast, garnets from water-undersaturated rocks have more complex zonation patterns with a characteristic intermediate decrease in pyrope and XMg. In some cases, garnets show an abrupt compositional change from core to rim, possibly due to water-undersaturation prior to HP metamorphism. Garnets from both water-saturated and water-undersaturated rocks show signs of intervening growth interruptions and core resorption. This results from bulk rock depletion caused by fractional garnet crystallisation.

The water content during burial significantly influences the physical properties of the subducted rocks. Due to enhanced garnet crystallisation, water-undersaturated rocks become denser than their water-saturated equivalents, facilitating the subduction of continental material. Although water-bearing phases such as phengite and epidote are stable up to eclogite-facies conditions in these rocks, dehydration reactions during subduction are lacking in water-undersaturated rocks up to the transition to the eclogite facies. Our calculations show that garnet zonation patterns strongly depend on the mineral parageneses during garnet growth and that certain co-genetic mineral assemblages cause distinct garnet zonation patterns. This enables one to interpret complex garnet growth zonation patterns in terms of garnet-forming reactions and water content during HP metamorphism, as well as to determine detailed P-T paths.

Key words: *dehydration; high-pressure metamorphism; Sesia Zone; subduction; thermodynamic modelling*

3.2 INTRODUCTION

Detailed pressure-temperature-time-(P-T-t) paths are diagnostic of the tectonic and mineralogical processes responsible for the rapid burial and exhumation of high-pressure (HP) rocks in subduction zones (Carswell and Zhang, 1999; Peacock and Wang, 1999; Liou et al. 2000; Aoya et al. 2003). In addition, the bulk chemical evolution, especially the volatile content of the buried rocks, plays an important role during subduction and exhumation processes, because it influences the physical properties of the downgoing slab. In devolatilisation reactions, volatiles can have a significant influence on seismicity and melt generation in subduction zones (e.g. Peacock, 1993; Schmidt and Poli, 1998). Furthermore, subduction of hydrous phases stable under mantle depth conditions contributes to volatile recycling into the mantle (Liou and Zhang, 1995; Scambelluri et al., 1995; Kerrick and Connolly, 2001). Many factors complicate the extraction of pressure-, temperature- and chemical information from high-pressure rocks. These factors include disequilibrium reactions, such as fractional crystallisation, the presence of relict mineral parageneses, devolatilisation during burial and polyphase metamorphic retrogression during exhumation. Due to the limitations of quantifying these disequilibrium conditions by conventional thermodynamic calculations, the mineralogical processes,

especially the prograde P-T trajectories of the subducted rocks, are often only very crudely defined.

Better constrained P-T paths and insight into the physico-chemical evolution of ultra-high-pressure (UHP)- and high-pressure (HP)- terranes can be derived by interpreting relict zonation patterns in prograde metamorphic minerals in the light of thermodynamic forward modelling that incorporates element- and fluid-fractionation during metamorphism. Garnet is best suited for these purposes because its composition is very sensitive to pressure and temperature changes, but also because cation diffusion in garnet is sufficiently slow to preserve compositional differences within grains. Thus, garnet growth zonation patterns are often used to constrain the P-T path of their host rock (Spear and Selverstone, 1983, Menard and Spear 1993; Okudaira, 1996; Ayres and Vance, 1997; Enami, 1998; Cooke et al., 2000; Escuder-Viruete et al., 2000), to determine the duration of metamorphic events (Lasaga and Jiang, 1995; Ganguly et al., 1996; Ganguly and Tirone, 1999; Perchuk et al. 1999) and to gain insight into crystal growth and transport mechanisms in metamorphic rocks (Hollister, 1966; Loomis, 1982; Cygan and Lasaga, 1982; Chernoff and Carlson, 1997; O´Brien, 1999; Spear and Daniel, 2001; Konrad-Schmolke et al., 2005). Many high- and ultrahigh-pressure rocks contain garnet with a growth zonation pattern reflected in core-overgrowth differences, both in inclusion assemblage and in major- and trace-element composition (O´Brien, 1997; Arenas et al, 1997; Zhang et al. 1997; Compagnoni and Hirajima, 2001). These chemical differences are reflected in very complicated zonation patterns, but the origin of these differences, although important for the petrological and geochronological interpretation, is poorly understood. In this study we investigate complex garnet zonation patterns from a large number of structurally characterised sample locations in order to gain insight into the prograde pressure-temperature-composition (PTX) evolution of high-pressure rocks from the Sesia Zone (Western Alps). This is done by comparing modelled garnet zonation patterns obtained by the method of Gibbs energy minimisation, with patterns observed in natural samples. In our calculations, we consider fractional garnet crystallisation, water fractionation as well as different mono- and poly-metamorphic P-T paths.

The Sesia Zone (SEZ) is of particular interest because it is one of the largest bodies of subducted and exhumed continental crust. It was subducted to ca.

60-65 km depths in late Cretaceous time (e.g., Duchene et al., 1997; Rubatto et al., 1999). Recent work has shown that the subduction of continental crust is a frequent process that might be responsible for element recycling within the mantle and accretion of lower crustal material to the overriding plate (e.g. Walsh and Hacker, 2004). The effects of a polymetamorphic history in subducted rocks can be especially well-studied in the SEZ, because it underwent Early Mesozoic rifting-related high-temperature metamorphism prior to its high-pressure Alpine metamorphic evolution (e.g. Lardeaux and Spalla, 1991; Rebay and Spalla, 2001). This strongly influenced the volatile content of the SEZ rocks prior to the Alpine high-pressure metamorphism and had a significant influence on the physical properties of the subducted rocks.

3.3 GEOLOGICAL SETTING

The SEZ is a large sliver of continental crust that underwent HP metamorphism during the Cretaceous to Tertiary collision of the Adriatic and European continental plates (e.g. Compagnoni et al., 1977; Dal Piaz et al., 1978). It is now exposed in the inner part of the Western Alpine arc (Fig. 3.1). Prior to subduction, the SEZ was part of the external continental margin of the Adriatic plate that was separated from the European continent by the so-called Piemont-Liguria Ocean. During plate convergence and subduction of this oceanic lithosphere, the Sesia rocks were tectonically eroded from the continental margin and subducted to a depth of about 60 km. Subsequent syn-convergent exhumation emplaced the SEZ at the top of the Western Alpine nappe pile (Dal Piaz et al., 1972; Paschier et al., 1981; Babist et al., Chapter 4). The SEZ is bounded in its footwall by ophiolitic remnants of the Piemont Ocean and to the SE by lower crustal rocks of the Southern Alpine Ivrea Zone. The Ivrea Zone only experienced an Alpine greenschist-facies metamorphism along its NW rim, adjacent to the Sesia Zone. Both contacts of the Sesia Zone are marked by first-order mylonitic shear zones that accommodated top-SE normal faulting as well as dextral strike-slip movement during the syn-convergent exhumation of the Sesia- and Piemont rocks (Wheeler and Butler, 1993; Reddy et al., 1999; Schmid et al., 1987).

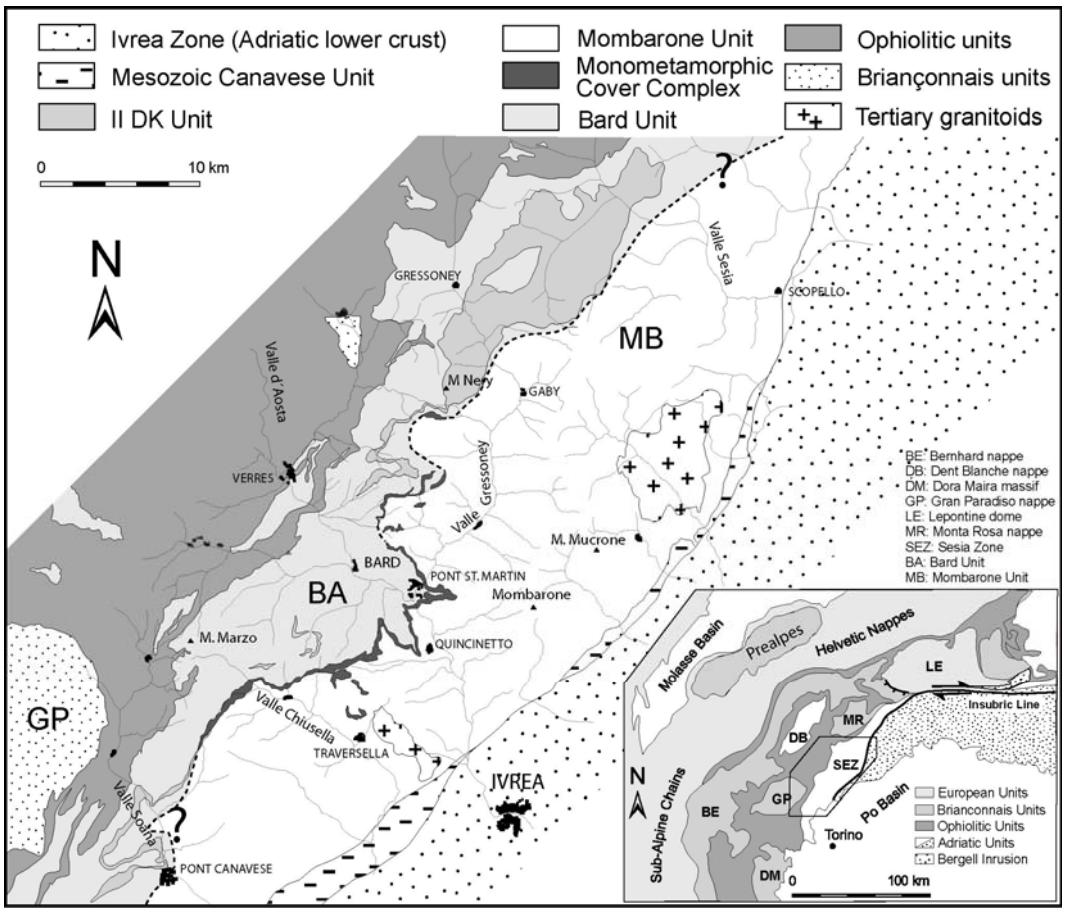

Fig. 3.1: Simplified geological map of the central Sesia Zone. The inset shows the position of the SEZ in the Western Alpine nappe pile.

3.3.1 Lithotectonic subdivisions

Lithologies in the SEZ mainly comprise metapelitic, meta-calc-pelitic and metagranitoid rocks intercalated with smaller slices of metabasites and subordinate lenses of carbonatic and quartzitic rocks. They can be divided into four units (Fig. 3.1):

(1) The *Mombarone Unit* contains the best preserved assemblages of Alpine HP metamorphism. This unit consists of large amounts of coarse grained, quartz-rich garnet-zoisite-omphacite-sodic amphibole-phengite gneiss and schist, basic eclogite and small lenses of omphacite-, phengite- and zoisite-bearing marble (Dal Piaz et al., 1972; Compagnoni and Maffeo, 1973; Gosso, 1977). In areas with a pervasive greenschist-facies overprint, such as in the northern part of the SEZ, metapelites are mostly retrogressed to epidote-biotite/chlorite-white mica-schists whereas metabasites are predominantly transformed to chlorite-albite-epidote-amphibole gneiss. Peak metamorphic conditions during Alpine

subduction are 500-600°C at pressures of 1.5-2.0 GPa (Dal Piaz et al. 1972; Compagnoni and Maffeo 1973; Reinsch, 1979; Desmons and O´Neil, 1978; Compagnoni et al., 1977; Oberhänsli et al., 1985; Koons, 1986; Vuichard and Ballévre 1988; Tropper et al., 1999; Zucali et al., 2002). Relics of pre-Alpine high-temperature minerals, abundant in other units of the SEZ, are scarce in the Mombarone Unit (Dal Piaz et al., 1972; Williams and Compagnoni, 1983).

(2) The *Bard Unit* forms the structurally lower part of the SEZ (Fig. 3.1). It is characterised by a strong Alpine greenschist-facies overprint (Pognante et al. 1987; Lattard 1975; Compagnoni et al. 1977; Stünitz, 1989) and consists mainly of fine-grained, biotite-bearing albite-white mica-epidote gneiss with minor intercalations of metabasic chlorite-calcic amphibole gneiss and subordinate phengite-bearing quartzites. Spalla et al. (1991) and Lardeaux and Spalla (1991) interpreted relics of omphacite found in the north-western part of the SEZ to reflect Alpine eclogite-facies metamorphism. Alpine peak metamorphic conditions have been 400-500°C at pressures between 1.1 and 1.5 GPa (e.g. Lardeaux and Spalla, 1991). Past authors have interpreted the contact to the Mombarone Unit to be a continuous metamorphic field gradient ranging from eclogite-facies conditions in the Mombarone Unit to greenschist-facies conditions in the Bard Unit (e.g. Passchier et al., 1981; Williams and Compagnoni, 1983). However, we found that the primary nappe contact is overprinted by a large subvertical mylonitic shear zone that accommodated transpressional shear and exhumed the Mombarone Unit with respect to the Bard Unit under retrograde blueschist- to greenschist facies conditions (Babist et al., in review).

(3) The *Bonze Unit*, first described by Venturini et al., (1994, their Monometamorphic Cover Unit), forms a band of Mesozoic, MORB-like metabasic rocks associated with smaller gabbroic lenses, manganese-rich quartzites and mica-bearing metacarbonate rocks. This unit can be mapped several tens of kilometres along strike. Peak metamorphic conditions in these rocks are around 550°C at 1.5 GPa (Venturini, 1995), somewhat lower than pressures found in the Mombarone Unit. This thin slice of rocks of possibly transitional oceanic-continental origin is interpreted to separate the Bard- and Mombarone-nappes that were juxtaposed during Late Cretaceous subduction (e.g. Venturini, 1995).

(4) The *II DK Unit*, interpreted to form the structurally highest member of the SEZ, consists of pre-Alpine granulite- and amphibolite-facies schist and gneiss (Carraro et al., 1970; Dal Piaz et al., 1971; Lardeaux et al., 1982). Most authors deduce peak temperatures between 700 and 800°C and pressures between 0.5 and 1.0 GPa for the pre-Alpine metamorphism (Lardeaux et al, 1982; Rebay and Spalla, 2001). Equilibration under blueschist-facies conditions occurred mainly along the tectonic contact to the Mombarone Unit (Gosso, 1977; Ridley 1989; Avigad, 1996). Alpine greenschist-facies overprinting of the II DK Unit is strain-dependent and affected mainly the smaller bodies of this unit in the central and southern part of the SEZ, as well as the structurally higher parts of the large II DK bodies (e.g. Compagnoni et al., 1977).

3.3.2 Structural framework

The Bard, Mombarone and II DK units described above individuated as nappes during initial accretion in late Cretaceous time (Babist et al., in review). This interpretation is based mainly on differences in the peak metamorphic conditions of these units, as well as on occurrence of Mesozoic sediments marking the nappe contacts. Structural analysis of the SEZ shows that the Mombarone Unit (Fig. 3.1) has a broad, open antiform that is bounded to the north-west by the steep blueschist-facies transpressive shear zone mentioned above. This shear zone effected initial exhumation of the Mombarone Unit from within the mantle (60 km depth) to 30-40 km depth within the accreted continental crust making up the upper plate of the active margin (Babist et al., in review). Mineral lineations and shear-sense indicators show an oblique S-block up exhumation of the Mombarone Unit with respect to the Bard Unit. Ridley (1989) and Avigad (1996) estimated 500-600°C at 0.9-1.4 GPa for this blueschist-facies deformation. This steeply dipping shear zone partly overprints the Bonze Unit.

Moderately dipping greenschist-facies top-down-to-E(SE) shear zones mark a low-angle extensional shear zone in the roof of the Mombarone unit that overprints HP rocks as well as the aforementioned blueschist-facies shear zone (Babist et al, in review). The northeastern part of the contact between the Sesia and Ivrea Zones is marked by brittle and ductile deformation associated with Oligo-Miocene exhumation along steeply dipping backthrusts (e.g. Schmid et al., 1987). Within the Bard Unit, the contact with the underlying Piemont ophiolites is

marked by a top-down-to-SE, mylonitic normal fault was active under retrograde greenschist-facies conditions. This fault is interpreted to have accommodated exhumation of Tertiary eclogite-facies oceanic remnants within the Piemont Unit (Wheeler and Butler, 1993; Reddy et al., 1999).

3.4 RESULTS

3.4.1 Sample locations and garnet zonation patterns

Garnets are widely distributed in the II DK, the Bonze and the Mombarone units. In the Bard unit, garnet is absent or restricted to a narrow contact zone with the Bonze and the Mombarone units. We sampled the main lithologies in the Bard, the Bonze and Mombarone units, as shown in Fig. 3.2. This sampling revealed a large variety of garnet zonation patterns in the Sesia rocks. Most of these zonation patterns show a significant chemical difference between core and rim compositions, although the transition between these compositions varies from very smooth in some samples to an abrupt, step-like change in composition in others. The zonation patterns can be divided into three different groups, independent of host-rock lithology (Fig. 3.2):

(1) The first group (white-background diagrams in Fig. 3.2) is characterised by increasing pyrope content and increasing XMg (Mg/Mg+Fe) component from core to rim. Although step-like zonation patterns with slightly decreasing Mg content in parts of the zonation pattern occur in a few cases, group I garnets generally show zonation patterns typical of prograde garnet growth in medium- to high-pressure rocks. Almandine generally increases from core to inner rim and decreases towards the outer rim. Grossular decreases from core to rim or, in some samples, remains constant throughout the entire profile. Spessartine always has a bell-shaped profile, with mole fractions between 0.2 and 0.5 in the inner cores.

(2) The second group (dark grey background) shows a characteristic step-like zonation pattern. The cores of group II garnets have a constant, sometimes slightly zoned almandine-rich, grossular-poor composition; the rims consist of almandine-grossular-rich garnet. At the abrupt transition between core and rim, garnet composition changes drastically with respect to all major elements. Pyrope content and XMg show a characteristic decrease followed by an increase towards

the outer rim. This drastic change in core-to-rim major element composition is opposite to the trend observed in the core-to-rim transition in group I garnets.

(3) The third group (light-grey background) shows a significant decrease in pyrope content and XMg over large parts of the profile at the transition between core and rim. In contrast to group II garnets, however, garnets from this group have smoother and smaller compositional gradients between core and rim. Group III garnets have extremely low spessartine contents and in most samples, all components show complex zonation patterns. Garnets from group II and group III very often occur within the same sample.

3.4.2 Spatial distribution of the different zonation patterns

Interestingly, there is a relationship between sample locality and garnet zonation pattern. Group I garnets only occur in rocks sampled near the contact between the Mombarone and Bard Units, as well as in rocks from the Bonze Unit (Fig. 3.2). Although the composition of group I garnets changes slightly between samples, depending on lithology, the shape of the zonation patterns (characteristic for this group) is almost identical. In contrast, samples from further within the Mombarone Unit contain group II and III garnets. Samples with garnets belonging only to group III are restricted to the internal parts of the Mombarone Unit.

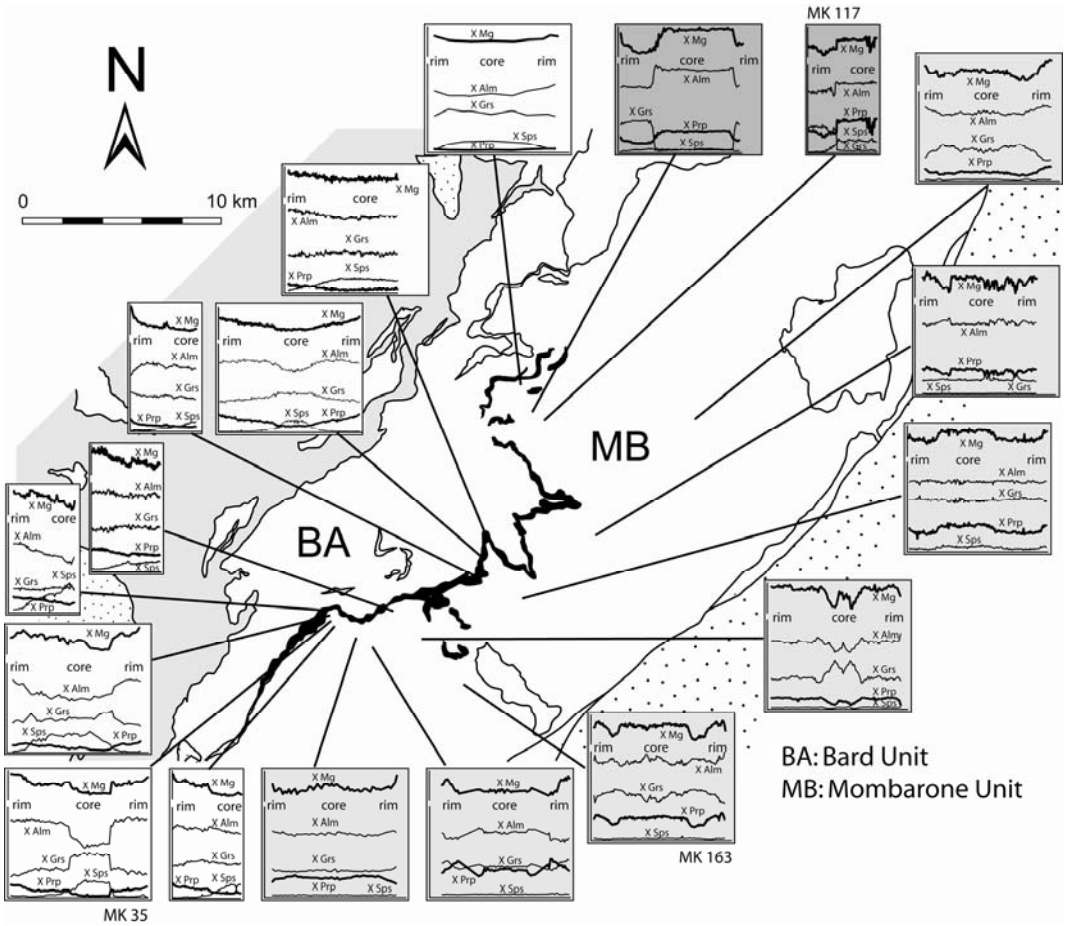

Fig. 3.2: Sample locations and compositional garnet profiles from the central Sesia Zone. Sample locations of group I garnets (white-background profiles) are restricted to the contact between the Mombarone and Bard Units as well as to the Bonze Unit. Group II (grey background) and III (light-grey background) garnets can only be found in samples from further within the Mombarone Unit. BA = Bard Unit; MB = Mombarone Unit.

3.4.3 Comparison of modelled and observed zonation patterns

In order to gain insight into the processes leading to the different characteristics of the zonation patterns, such as abrupt compositional changes and significantly decreasing Mg content, and to reconstruct parts of the prograde metamorphic history of the eclogitic rocks in the Sesia Zone we carried out thermodynamic forward modelling of garnet zonation patterns along different P-T-paths and with different fractionation scenarios. We modelled garnet zonations patterns for all investigated samples. In the following we show the results for three representative samples. The first sample contains garnets belonging to group I, the second contains garnets from group II and III, and the third sample contains group III garnets only.

3.4.3.1 Sample MK 35 (group I garnets)

Sample MK 35 is a strongly foliated, quartz-rich metatonalitic rock sampled in the blueschist facies mylonite zone between the Mombarone and Bard units (Fig. 3.3). The Alpine high-pressure mineral assemblage is strongly affected by a retrograde greenschist facies overprint, resulting in the disequilibrium mineral assemblage biotite-chlorite-garnet-calcic amphibole-sodic amphibole-albite-epidote-phengite-quartz. Although relics of omphacite can be found in this sample, it is mostly retrogressed to white mica, albite, calcic amphibole and minor chlorite. Sodic amphibole is either completely, or at the rims, replaced by biotite, chlorite and calcic amphibole. Garnets in sample MK 35 form clasts in the well-developed mylonitic foliation. The garnet clasts range from small fragments up to hypidiomorphic grains up to 1.5 mm in diameter. Epidote and quartz are the most common inclusion phases in the cores of group I garnets, whereas inclusions in the rims, typically located in concentric inclusion zones, comprise epidote, rutile and quartz (Fig. 3.3a). Large (>0.5 mm) grains are very often atoll-like in shape with resorbed cores, entirely replaced by phengitic mica, epidote and/or quartz (Fig. 3.3a). In some cases, as shown in the backscattered electron (BSE) image in Fig. 3.3a, which displays a garnet from this sample with a darker, irregularly formed core overgrown by a lighter mantle and a darker outer rim, newly formed garnet with the same composition as the brighter mantle region can be found within the resorbed cores (arrow in Fig. 3.3a). Fig. 3.3b shows a group I garnet from this sample with an euhedral core, that is only weakly affected by resorption (arrow). The white line represents the position of the compositional core-to-rim profile in Fig. 3.3c. The compositional profile shows a step-like zonation pattern with an almandine-grossular-rich core and an almandine-rich mantle and rim. Apart from a small region between core and mantle, pyrope as well as XMg is steadily increasing. Spessartine shows a typical bell-shaped zonation with mole fraction values around 0.2 in the core and a slight intermediate increase at the core-rim transition. The grossular content changes from between 0.35 to 0.4 in the core to values around 0.3 at the inner rim, decreasing to mole fraction values about 0.2 at the outer rim. Almandine content increases from 0.45 in the core to 0.8 at the inner rim, followed by a slight decrease to 0.7 near the outer rim.

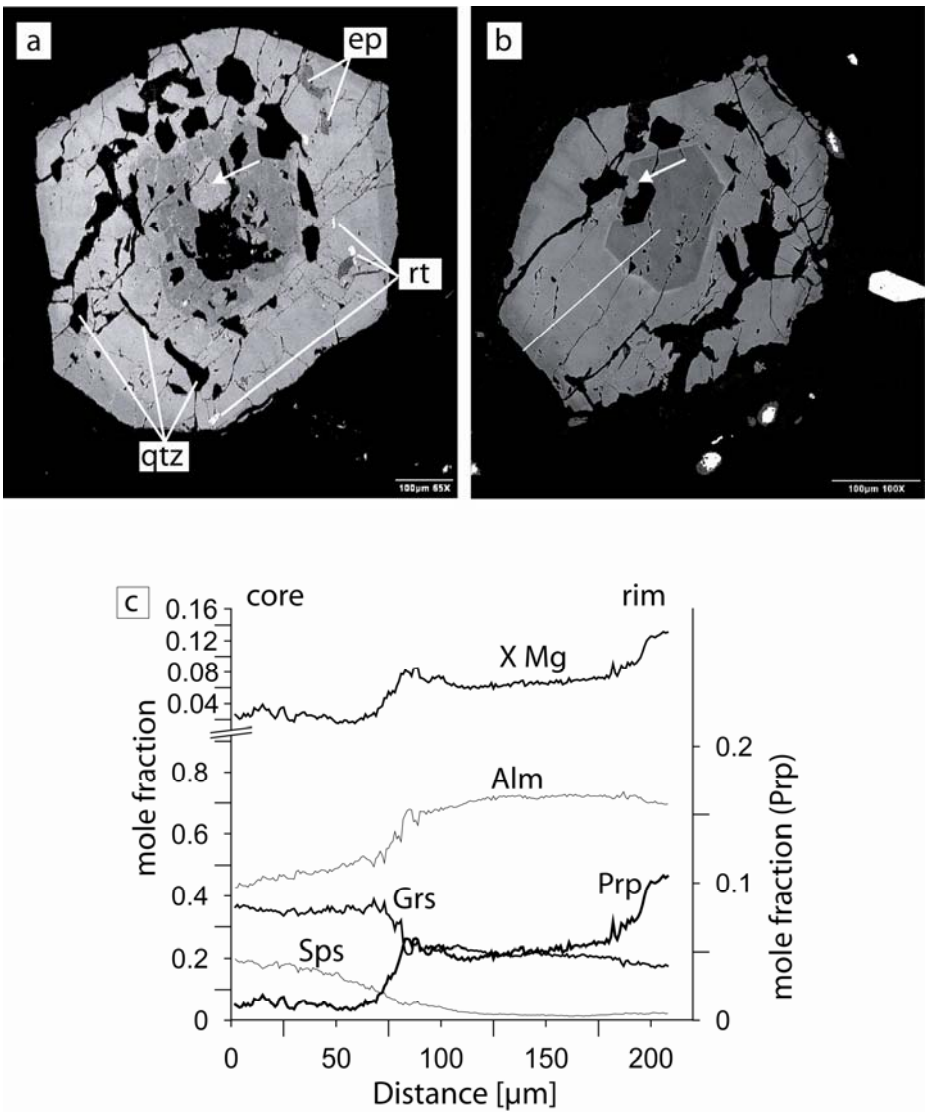

Fig. 3.3: a) Backscattered electron image of an atoll-like group I garnet from sample MK 35. A partly resorbed dark core is overgrown by a lighter mantle, followed by a darker rim. The arrow marks new mantle material grown within the core. Inclusions of epidote, quartz and rutile are often aligned in concentric trails. b) Group I garnet from the same sample but with unresorbed core. Resorption is indicated only by small embayments filled with mantle material (arrow). The core-mantle-transition is highlighted by a small bright rim, caused by the enrichment of trace elements; c) Compositional profile along the white line in a). Typically, group I garnets are characterised by steadily, sometimes step-like increasing pyrope content and increasing XMg.

3.4.3.2 Sample MK 117 (group II and III garnets)

Sample MK 117 is a quartz-rich zoisite-garnet-sodic amphibole-calcic amphibole-phengite gneiss with a strong foliation, defined by white mica and amphibole. The foliation in this sample is parallel to that in the mylonite zone, but the sample location is further within the Mombarone Unit than that of the previous sample (Fig. 3.2). Relic omphacitic pyroxene can be found in pseudomorphs consisting of albite, white mica, chlorite and calcic amphibole.

Apart from the almost completely replaced omphacite, the high-pressure assemblage is only partly replaced by greenschist facies minerals. Retrogression is mostly restricted to the grain edges of sodic amphibole, garnet and phengite. Garnets in this sample belong to group II and III and show a strongly bimodal grain size distribution. Whereas group II garnets are between 1 and 5 mm in size and have irregular grain shapes, garnets belonging to group III are smaller (up to 1 mm) and have subhedral but also rounded and irregular shapes. Both types form clasts within the mylonitic foliation. Grain boundaries to other syn-metamorphic phases sometimes have reaction rims.

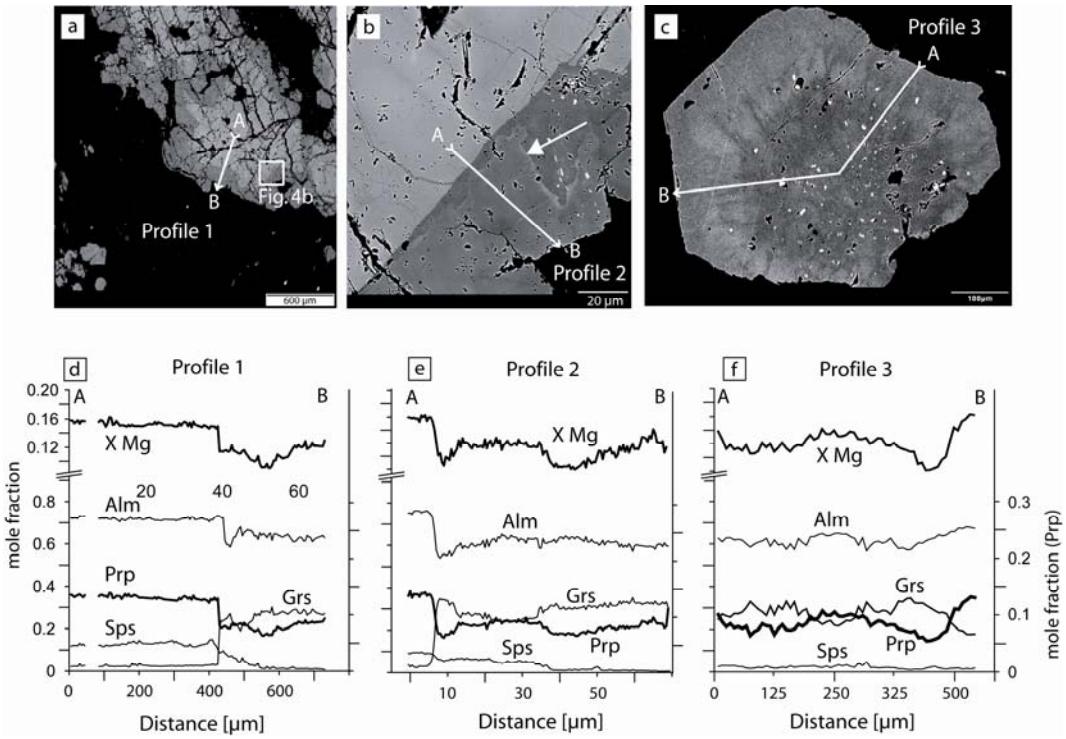

Fig. 3.4: a) Backscattered electron image of a cluster of group II garnets. Light garnet cores that often show near-euhedral grain shapes are overgrown by darker rims. The rectangle marks the close-up view in b); b) Detailed view on the darker overgrowth. Two different growth zones are visible: a darker, irregularly-shaped, sometimes inclusion-rich inner zone is overgrown by a thin light band (arrow), followed by a darker overgrowth. c) Group III garnet from the same sample. The darker core shows numerous epidote, quartz and rutile inclusions. The lighter mantle and the rim are inclusion-poor or –free. d) Compositional profile of a group II garnet measured along the white line in a). e) Detailed compositional profile across the overgrowth in group II garnets shown in b) Note the complex zonation pattern in the darker overgrowth (profile 2). f) Compositional profile across the group III garnet in c.

Garnets belonging to group II have inclusion-poor euhedral, sometimes complexly formed cores followed by inclusion-rich rims (Fig. 3.4a and b) containing numerous epidote and rutile inclusions that are often concentrically

arranged between core and inner rim. Group III garnets in this sample are mostly euhedral but sometimes show signs of resorption along the rims. They have numerous epidote and rutile inclusions concentrated in the core (Fig. 3.4c).

The BSE image in Fig. 3.4a shows a cluster of garnets from group II. Clearly visible is a bright core, overgrown by a darker rim. The image in Fig. 3.4b shows a closer view of the garnet overgrowth. The position is marked by the white rectangle in Fig. 3.4a. The close up image shows that the core is heavily truncated by cracks, filled with garnet rim material. Associated with these cracks is a diffusional relaxation of the garnet core composition indicated by the darker areas around the filled cracks (Fig. 3.4b). The darker rim has an inclusion-rich zone shown on the right side of the image (bright spots are rutile inclusions). Interestingly there is an irregularly-shaped small overgrowth with a slightly darker colour followed by a brighter zone (arrow in Fig. 3.4b) that cannot be found in all regions around the core. Fig. 3.4d shows a compositional core-to-rim profile across a large group II garnet (white line in Fig. 3.4a). The profile is characterised by a significant difference in core and rim composition. In the core, almandine content is constant between mole fractions of 0.71 and 0.75, pyrope and spessartine are between 0.1 and 0.16 and grossular is extremely low between 0.01 and 0.05. Towards the rim this composition changes abruptly. Fig. 3.4e displays a detailed compositional profile across the transition from core to rim. Here it can be seen that in the overgrowth almandine drops to values around 0.6, increases slightly again to 0.7, in some cases followed by a slight decrease to 0.65. Pyrope decreases at the core-overgrowth transition from 0.12 in the core to 0.08 in the innermost rim, decreases after a small plateau to values around 0.06, followed by a steady increase towards the outermost rim. The zonation pattern of grossular is also quite complex. At the core-rim transition grossular mole fraction rises to around 0.3 followed by an intermediate depression and is slightly decreasing towards the outer rim. Interestingly there are two zones, where the pyrope content shows small minima (Fig. 3.4e). One after the transition from core to rim, associated with an increase in grossular content and a second one half way towards the outer rim. Spessartine shows a slight increase at the core-rim transition (Fig. 3.4d) but generally decreases from core to rim in two distinct plateau-like zones (Fig. 3.4e).

Group III garnets in this sample mostly occur as single grains in the matrix, but in few cases was found as inclusion in omphacite as well. Textural relations of matrix garnet suggest equilibrium parageneses with phengite and sodic amphibole. The profile in Fig. 3.4f shows the compositional variation along the white line in Fig. 3.4c. Although all investigated group III-garnets in this sample are extremely Mn-poor, Spessartine often shows a preserved zonation pattern, with slightly increasing Mn-content at the inner rim and towards the outermost rim (Fig. 3.4f), possibly the result of Mn back-diffusion due to garnet resorption. Almandine and grossular show the largest compositional variations and most complex zonation patterns. Almandine decreases from mole fraction values around 0.7 in the inner core to values around 0.55 at the outer mantle and increases again to 0.7 at the outermost rim. The molar fraction of grossular shows the opposite pattern. It increases from core to outer mantle from 0.2 to 0.4 and decreases to values below 0.2 at the outer rim. Both, pyrope content and XMg show similar trends as the almandine pattern. They decrease from core to inner rim with a minimum at the transition between inner and outer rim and a strong increase towards the outer rim (Fig. 3.4f).

3.4.3.3 Sample MK 163 (group III garnets)

Sample MK 163 is a coarse grained, rutile-bearing zoisite-garnet-sodic amphibole-phengite-omphacite- gneiss with a weak foliation defined by large phengite, sodic amphibole and omphacite grains. The sample location lies well within the Mombarone Unit (Fig. 3.2). Garnets in this sample are of group III type and mostly euhedral. In many cases garnets form cluster of several single grains that amalgamated in a late growth stage (Fig. 3.5a). Single garnet grains are between 0.1 and 0.5 mm in diameter and often appear as inclusions in large omphacite grains (Fig. 3.5a) as well as in the matrix. Grain boundaries between garnet and omphacite are often affected by small retrograde albite rims resulting from pyroxene breakdown (Fig. 3.5a). Textural relations of matrix garnet suggest equilibrium parageneses with phengite and sodic amphibole. Garnets in this sample range from inclusion-free to grains with inclusion-rich cores and inclusion-poor rims. If present, the inclusions consist of quartz, epidote and/or rutile. Almandine has the highest values slightly outside the innermost core (Fig. 3.5b). From there it decreases from 0.6 to about 0.5 at the transition from core to rim, followed by an intermediate high with values around 0.6 at the inner rim and

an increase towards the outermost rim. Grossular content shows the opposite pattern in the core and at the outer rim, but interestingly has a parallel pattern at the intermediate rise in the inner rim.

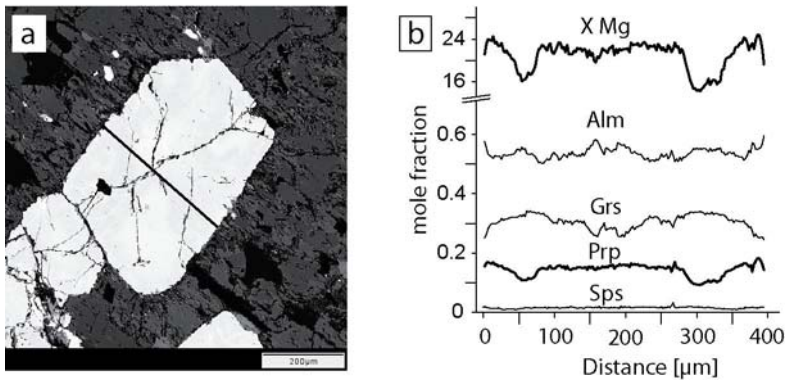

Fig. 3.5: a) Backscattered electron image of a group III garnet enclosed in a large omphacite crystal. The dark rim around the garnet crystal is retrograde albite formed by the decomposition of omphacite during exhumation; b) The compositional profile typically shows a complex zonation pattern with an interim decrease in pyrope content and XMg. Interestingly Almandine and Grossular patterns show opposite trends in the core and parallel trends in the mantle region (see text for discussion).

In the inner core grossular forms a small plateau at about 0.3 followed by an increase to values around 0.35 at the transition from core to rim. In the inner rim grossular shows the same intermediate rise as observed in the almandine pattern but decreases rapidly towards the outer rim to about 0.2. The zonation pattern of pyrope shows a large plateau in the core at values around 0.15. This plateau coincides with the region of contrary compositional behaviour of almandine and grossular. At the core to rim transition pyrope content decreases rapidly, followed by an increase to values of 0.2 at the rim. In this region Pyrope shows the opposite trend of Almandine and Grossular.

3.4.3.4 Thermodynamic forward modelling

The technique of Gibbs energy minimisation, utilising internally consistent thermodynamic datasets and relevant activity-composition models, allows the determination of equilibrium mineral modes and compositions for a fixed bulk composition at any pressure-temperature condition (e.g. de Capitani and Brown, 1987; Connolly, 1995; Spear and Menard, 1989). In this study we used the internally consistent dataset of Holland and Powell (1998) and various solid

solution models. Both, the thermodynamic dataset as well as the solid solution models can be found in the appendix.

Considering that a proportion of the volume of material in slow diffusing phases, such as garnet, as being fractionated out of the effective (i.e. reacting) bulk rock composition, we divided a P-T interval of interest into regularly spaced P-T points, at each of which we calculate the thermodynamic properties of the chemical system. Modelling fractional crystallisation involved modifying the chemical composition between two points by removing the amount of each component incorporated in garnet from the bulk rock composition, provided that garnet forms a stable phase in the assemblage. In contrast, in cases where garnet resorption was assumed, fractionated material was returned to the reacting bulk rock composition. With this gradually changing bulk rock composition, it is possible to model the thermodynamic properties of the rock system affected by fractional crystallisation of various minerals along a P-T path of interest. To model zonation patterns we calculated the moles of garnet and its composition produced over the P-T interval between two points. The amount of garnet is converted into a volume and a radial growth increment. Garnet composition is then plotted as a garnet zonation pattern by assuming a spherical grain shape. Further, we considered the effect of devolatilisation by progressively removing free water from the system in all calculations (cf. Konrad-Schmolke et al., 2005).

In order to reconstruct the P-T evolution of the samples as well as the influence of varying water contents of the host rock on garnet composition we modelled garnet zonation patterns for the specific bulk rock compositions of the samples along different P-T trajectories starting at the same PT conditions of 400°C at 0.5 GPa (Fig. 3.6) and different water fractionation scenarios.

(1) The first P-T path (path 1) leads into the epidote amphibolite facies, marked by rapidly increasing temperatures during the first part of the subduction path followed by a segment with little heating at increasing pressures.

(2) The second trajectory forms a straight line from 400°C at 0.5 GPa to 550°C at 2.0 GPa (path 2).

(3) The third path (path 3) displays the situation in a fast subduction zone with rapidly increasing pressures at relatively low temperatures and increasing temperatures at greater depths.

(4) Additionally we modelled a pre-Alpine high-temperature path leading to peak conditions of 750°C at 0.8 GPa followed by a high-pressure path.

To get insight into the influence of water content and water fractionation on the physico-chemical properties of the samples we modelled three different types of water-fractionation scenarios:

(i) Water-saturated conditions; in this case we calculated the thermodynamic parameters assuming water to be always present as a free phase along the modelled P-T path.

(ii) Dehydration-only conditions; the rock is assumed to be initially water-saturated, but the amount of free water, if stable is subtracted from the bulk composition at every calculated step.

(iii) Water-undersaturated conditions; the rock initially contains less water than necessary to form a free fluid phase.

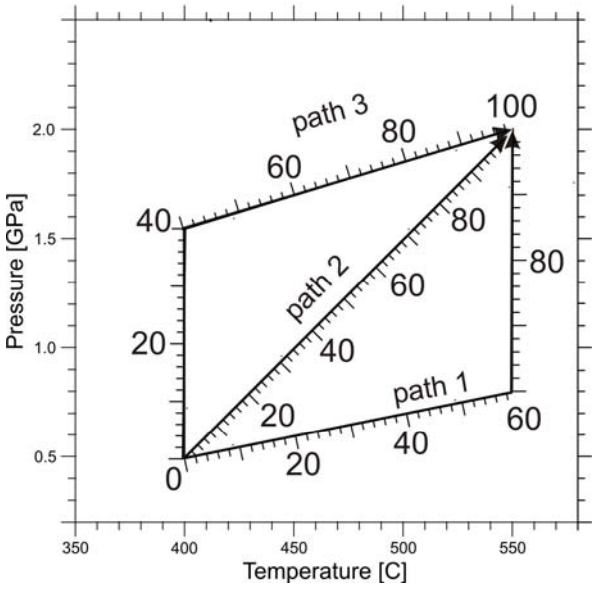

Fig. 3.6: Modelled P-T paths and calculated P-T increments along the trajectories.

3.4.3.5 MK 35 (group I garnets)

Fig. 3.7 shows the modelled garnet zonation patterns along the three different P-T paths for water-saturated (Fig. 3.7a) and dehydration-only (Fig. 3.7b) conditions. The different P-T trajectories as well as the different water fractionation conditions lead to significant differences in the garnet zonation

patterns. Although in all cases garnet growth occurs in at least two stages, indicated by the growth interruptions and the rapid compositional changes from core to rim, there are characteristic features that can be used to constrain the metamorphic evolution of the natural sample. In case of water-saturated conditions the modelled growth zonation patterns show distinct growth interruptions at the core-rim transition, resulting in an overgrowth zone characterised by abrupt changes in garnet composition (Fig. 3.7a).

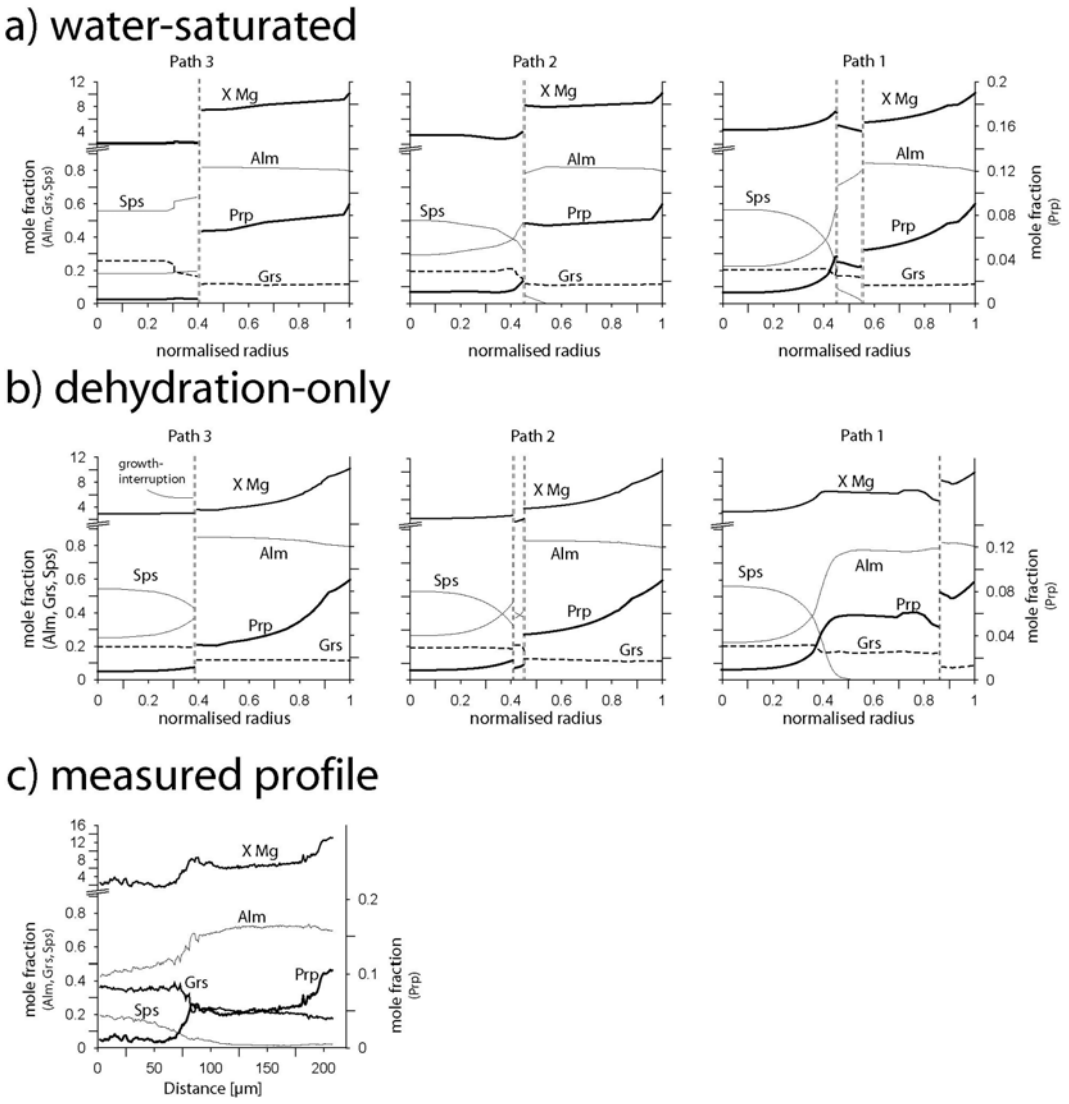

Fig. 3.7: a) Modelled garnet zonation patterns for sample MK 35 assuming a water-saturated host rock along the three P-T trajectories shown in Fig. 3.6. The modelled pattern for path 2 closely resembles that of the natural sample. The compositional changes as well as the growth interruption that enables core-resorption can be predicted; b) Modelled garnet zonation patterns for the same P-T paths as in a), but assuming dehydration during metamorphism. In this case the naturally observed pattern is best reproduced by modelling along path 1; c) Naturally observed core-rim profile for comparison.

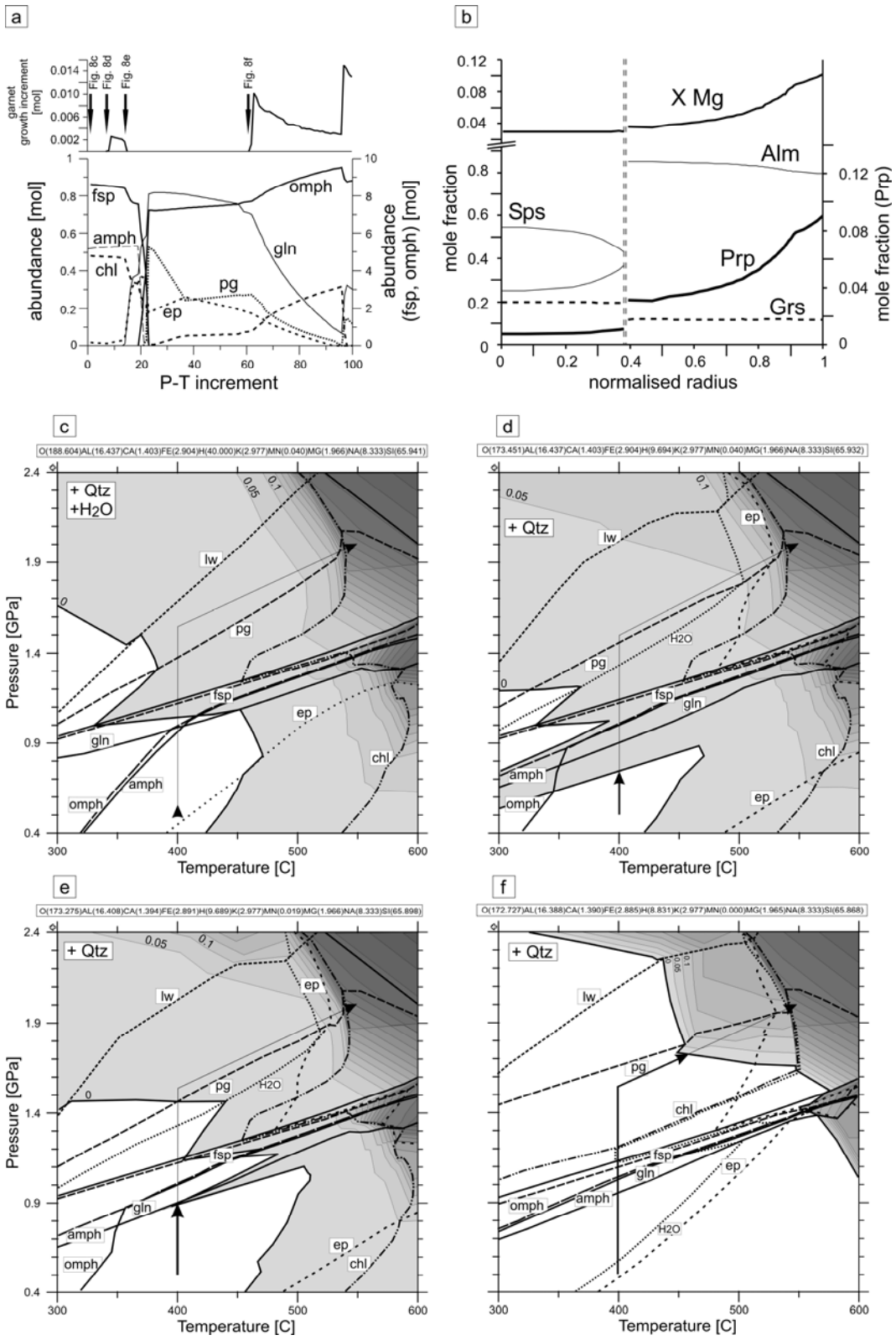

Fig. 3.8: The effect of fractional crystallisation on garnet growth. a) Garnet growth increment and modal abundance of garnet influencing phases calculated along P-T path 3. The arrows mark the P-T increments for which the bulk composition is used to calculated the pseudosections (c-f). b) Calculated core-to-rim garnet composition along path 3. c-f) pseudosections and contours for molar abundance of garnet calculated for progressively depleted bulk rock compositions according to the fractionation along path 3. Darker colours indicate higher values. See text for further discussion.

The reason for the interruption of garnet growth along the P-T trajectory as well as changes in the modal amounts of minerals that affect garnet growth are displayed in Fig. 3.8. The modal abundance plot in Fig. 3.8a as well as the pseudosections in Fig. 3.8c-f are calculated along path 3 assuming water fractionation. Fig. 3.8a shows that garnet grows in three stages, one of which occurs in the greenschist-facies (between P-T increment 8 and 15), the second in the blueschist-facies (between increment 60 and 95) and the third starts with the transition to the eclogite facies (around increment 95). The first garnet growth in the greenschist-facies occurs at the expense of plagioclase and chlorite indicated by the decreasing modal amounts of these phases in Fig. 3.8a. The resulting garnet composition is almandine- and spessartine-rich (Fig. 3.8b), typical for greenschist-facies garnets. Between the first and the second growth stage, there is a large P-T segment, where no new garnet material is produced (between increments 16 and 60; Fig. 3.8a).

The development of growth interruptions can nicely be demonstrated by a sequence of pseudosections (Fig. 3.8c-f) that are calculated for bulk rock compositions that are progressively depleted by fractional crystallisation and water fractionation. The diagrams are calculated for the bulk rock compositions according to the P-T increments labelled by the arrows in Fig. 3.8a. The first diagram (Fig. 3.8c) displays the phase relations and the modal amount of garnet (contours) for this sample assuming water saturated conditions and an undepleted bulk rock composition at the start of the forward modelling (first arrow in Fig. 3.8a). For simplicity only those zero mode lines are shown that influence garnet growth. Mineral labels are marked on the "present" side of the zero mode lines. The contours for the garnet mode indicate that garnet abundance is quite low up to temperatures between 450°C and 550°C depending on pressure and increases rapidly at the transition to the eclogite- and garnet-amphibolite-facies, caused by the breakdown of chlorite (chl) towards higher temperatures above 1.6 GPa and the formation of epidote (ep) towards higher pressures at temperatures around 600°C. Interestingly, the stability field of garnet reaches well into the greenschist-facies P-T field between 1.0 and 1.3 GPa at temperatures around 400°C.

The pseudosection in Fig. 3.8d is calculated for the bulk rock composition at the onset of garnet growth (second arrow in Fig. 3.8a). Although the phase relations of most minerals are similar to those in the first diagram, the stability

field of garnet is significantly enlarged at greenschist-facies conditions compared to the diagram in Fig. 3.8c caused by water fractionation during the sample's prograde metamorphic evolution between 0.5 and 0.7 GPa. Due to the smaller water content there is a P-T field (above the zero mode line of H_2O), where the sample can become water undersaturated with increasing pressure. The third diagram is calculated for the bulk rock composition at the last stage of the first garnet growth stage (arrow 3 in Fig. 3.8a). Due to fractional garnet crystallisation the stability field of garnet becomes smaller and increasing pressure during metamorphism leads the sample out of the garnet stability field. The stable assemblage after the first garnet growth stage is feldspar (fsp)+sodic amphibole (gln)+calcic amphibole (amph)+epidote (ep)+quartz, garnet is only present as a fractionated phase. Further garnet growth in the lower blueschist-facies field is then depending on reaction kinetics, that enable element recycling from the fractionated garnet clasts back into the reacting bulk rock composition. If all fractionated material remains in the garnet crystals produced so far, garnet is not part of the stable assemblage until the rock reaches the blueschist- to eclogite-facies transition, as shown in the diagram in Fig. 3.8f, which is calculated for the bulk rock composition at the onset of the second garnet growth stage.

As mentioned above, these garnet growth interruptions might be characteristic for certain shapes of the P-T trajectory. In case of garnet growth along path 1, two growth interruptions lead to a three-stage garnet growth, a feature that cannot be observed in the natural sample (Fig. 3.7c). Also, the pattern calculated along path 3 does not resemble the measured profiles because neither the increasing spessartine content nor the plateau-like almandine pattern in the core can be seen in the natural samples. In contrast, the pattern modelled along path 2 very closely resembles that in sample MK 35. The slight decrease in pyrope content associated with an increase in grossular prior to the growth interruption can be observed in the natural sample. Also the slight decrease in pyrope and XMg after the compositional break matches the natural pattern well. The growth interruption predicted by the model is also in agreement with the resorption structures and the intermediate spessartine increase that can be observed at the core-rim transition in the natural samples or is indicated by the resorbed cores of the atoll-like garnets in this sample (Fig. 3.3a). Interestingly, in case of the dehydration-only model (Fig. 3.7b), the pattern modelled along path 3

is in best agreement with the natural one. In this case the models for path 1 and 2 do not produce zonation patterns resembling those from sample MK 35. Nevertheless, all calculations show, that group I garnets, at least those in sample MK 35, grew in the presence of a hydrous fluid phase.

3.4.3.6 MK 117 (group II garnets)

Fig. 3.9 shows the modelled garnet zonation patterns along the three different paths for sample MK 117 and dehydration-only conditions. Starting with water-saturated conditions the rock followed paths 1-3 undergoing fractional garnet crystallisation and water fractionation as in the models before.

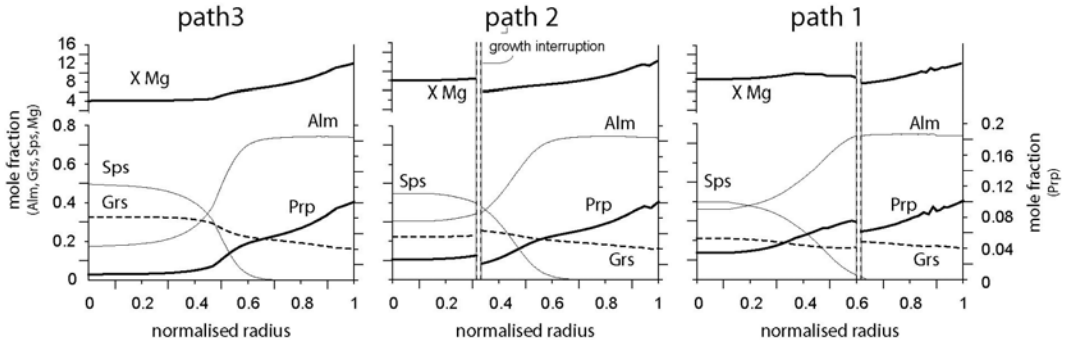

Fig. 3.9: Modelled garnet zonation patterns for sample MK 117 (garnet II) for the different P-T trajectories assuming dehydration during metamorphism. Obviously none of the modelled patterns that are very similar to those in Fig. 3.7 shows the same characteristics as the natural sample.

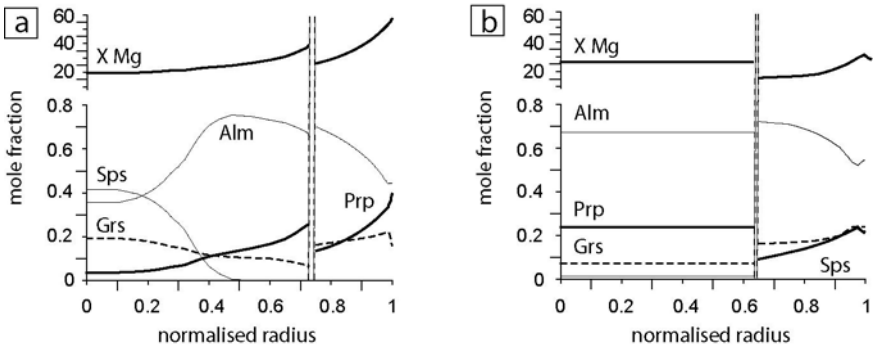

Fig. 3.10: a) Modelled garnet zonation pattern assuming polymetamorphic garnet growth. The internal part of the profile is the result of a prograde evolution up to upper amphibolite facies conditions. The overgrowth displays the high-pressure garnet overgrowth; b) Modelled pattern assuming complete equilibration of the entire grain at upper amphibolite facies conditions, followed by a high-pressure evolution along path 2. In both cases, the HP overgrowth starts with slightly higher Almandine content, a feature not observed in the natural sample.

It is obvious that none of the modelled zonation patterns in Fig. 3.9 resembles the compositional zonation of the garnets from sample MK 117. In all cases initial garnet growth starts with spessartine-almandine-rich compositions followed by a smooth transition to almandine-grossular-rich garnet rims. The abrupt compositional break at the core-overgrowth transition cannot be observed in these calculations. Thus, the grossular-poor core of the group II garnets is of different origin.

As mentioned above, the rocks of the Sesia Zone underwent a pre-alpine high temperature metamorphism with peak conditions around 750°C at 0.6-1.0 GPa. Thus the possibility of the preservation of a polymetamorphic garnet growth is evident. To reconstruct garnet growth in such a polymetamorphic scenario we modelled garnet growth for two different polymetamorphic P-T paths. Fig. 3.10a shows the modelled zonation pattern along a prograde high temperature path from 400°C at 0.5 GPa to peak temperatures of 750°C at 0.8 GPa followed by high-pressure path 3.

Although several authors report pre-Alpine HT garnets with well-preserved chemical zonation patterns it is most likely that the growth zonation in these HT garnets are largely equilibrated at amphibolite or granulite facies conditions, because volume diffusion in garnet becomes significantly fast at temperatures above 550°C. To account for that we calculated the garnet zonation pattern with a core composition equilibrated at 750°C at 0.8 GPa, followed by an Alpine overgrowth along path 3. The result is shown in Fig. 3.10b. The almandine-pyrope-rich core is overgrown by an almandine-grossular-rich rim that shows the same compositional trend as the profiles in Fig. 3.9a. As in the profile shown in Fig. 3.10a, the first HP overgrowth shows slightly higher Almandine contents than the garnet equilibrated at upper amphibolite facies. Both zonation patterns calculated for a polymetamorphic evolution show significant differences to those observed in the natural sample. Although the relative changes in grossular and pyrope contents are similar to those in the natural sample, the higher almandine content of the first overgrowth as well as the compositional trends in the HP overgrowth do not resemble those in the sample.

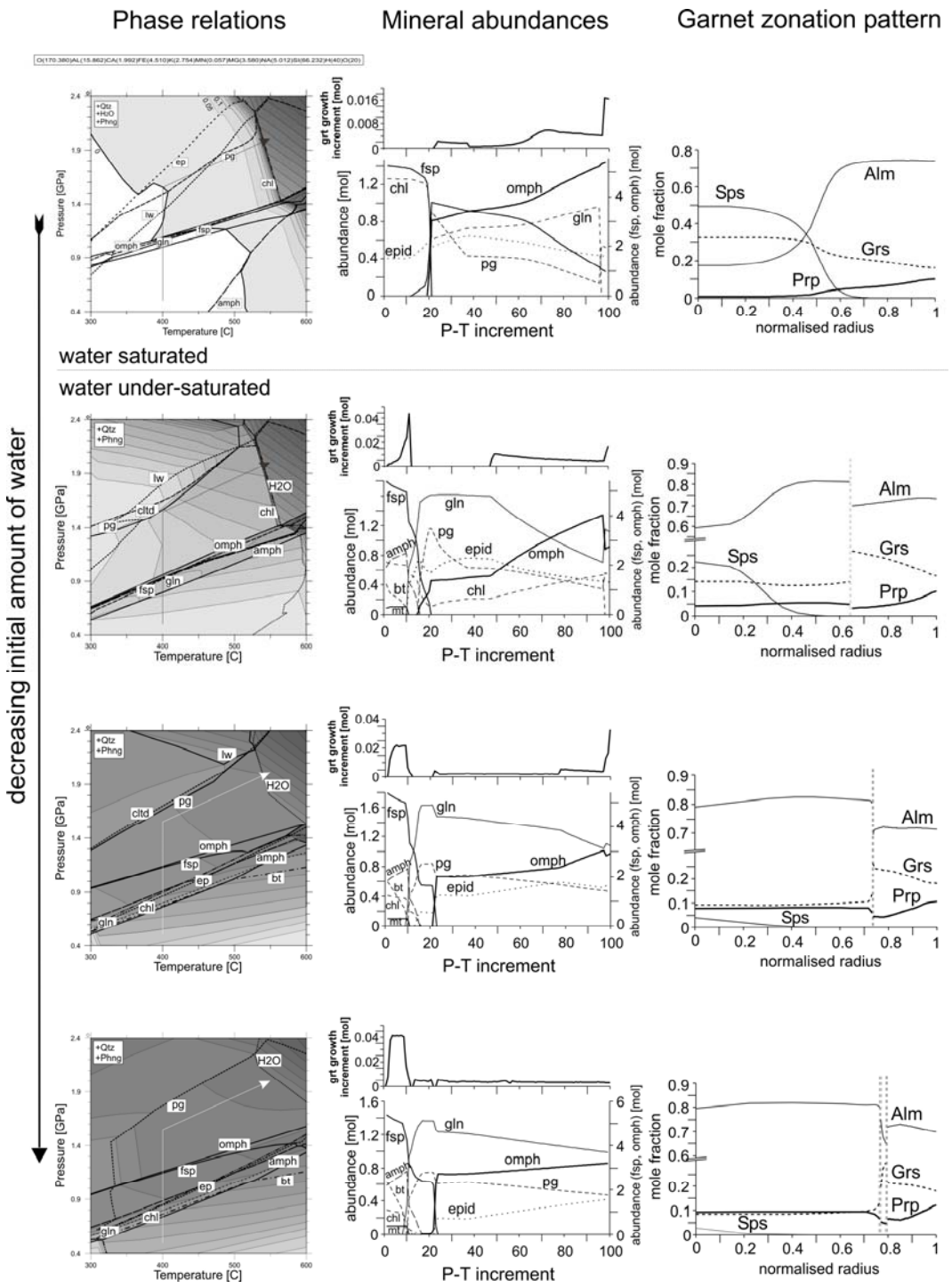

Fig. 3.11: Pseudosections with garnet molar isopleths, garnet growth increments and garnet zonation patterns calculated along path 3 with decreasing initial amount of water from top to bottom. The diagrams in the first line are calculated assuming water saturation (40 moles). The following diagrams are calculated with 12.5, 10 and 9 moles of water respectively. Decreasing initial amount of water in the system has significant influence on the amount and the composition of garnet. See text for further explanation.

Apart from relict cores of metamorphic minerals, the pre-Alpine HT metamorphism might have influenced the initial water content of the Sesia rocks prior to the HP metamorphic overprint. Therefore we modelled garnet growth

along the HP trajectory starting with different initial water contents. This yielded interesting, quite unexpected results: Fig. 3.11 shows calculated pseudosections for that sample, the modelled mineral abundances as well as garnet zonation patterns calculated along path 3 for different initial water contents of the host rock. The uppermost diagrams in Fig. 3.11 display water saturated conditions, whereas the following diagrams are calculated with increasing water-undersaturation. Water-undersaturation has a strong influence on the amount of garnet present at certain P-T conditions, on the initial garnet composition as well as on the phase assemblage during the metamorphic evolution. As indicated by the pseudosections, garnet growth starts at lower temperatures and the amount of garnet is much higher in rocks with low water contents than in water-saturated rocks.

Due to mass balance constraints this results in a much lower spessartine content of the garnet cores. Interestingly the grossular content is also extremely low in these garnets, a result of the different equilibrium mineral assemblage at greenschist facies conditions. In case of water-saturated conditions, initial garnet growth occurs mainly at the expense of chlorite. At water-undersaturated conditions garnet growth starts in the presence of calcic amphibole and occurs mainly at the expense of biotite (Fig. 3.11). This difference in the equilibrium mineral assemblage, caused by limited water-availability, leads to significant changes in garnet composition and growth history. Remarkable is also the complex pattern in the rim overgrowth shown in the lowermost diagram, which is a result of the short growth interruptions at the core to rim transition. The close-up BSE image in Fig. 3.4b shows the lighter core with straight grain boundaries that are almost unaffected by resorption that is overgrown by a small darker rim. This overgrowth shows a rapidly changing thickness and is marked by a thin light zone (arrows). The naturally observed compositional profile across the rim overgrowth (Fig. 3.4d and e) shows that the composition of the small dark zone is significantly different from the rest of the overgrowth. Almandine and pyrope show a characteristic minimum and grossular has an intermediate maximum in the small overgrowth zone. This complex chemical zonation as well as the two growth interruptions, which cause the complex zonation pattern in the garnet rim, can be predicted by the calculations assuming water-undersaturated conditions at initial garnet growth (lowermost diagrams in Fig. 3.11).

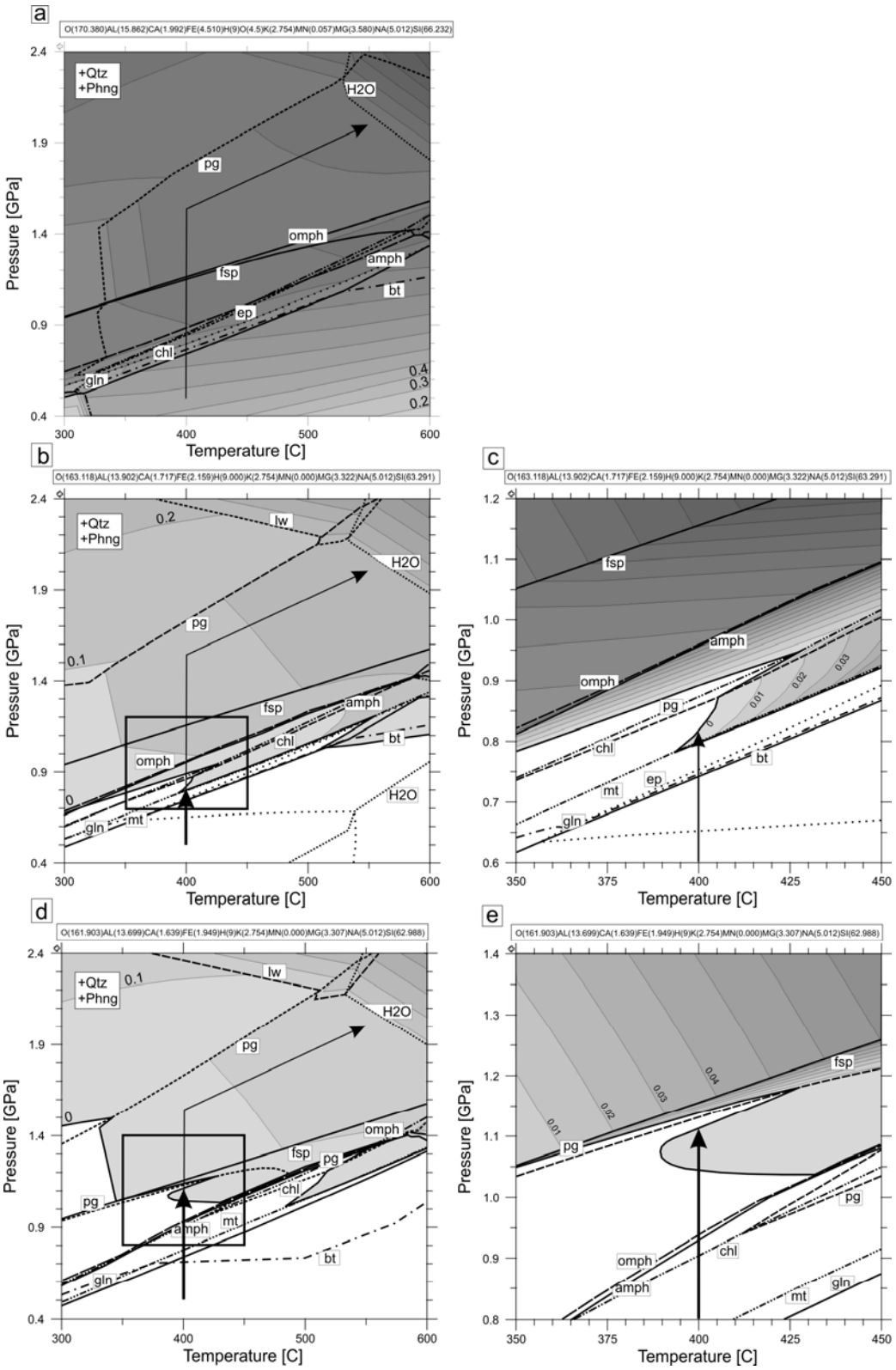

Fig. 3.12: a) Pseudosection and garnet molar isopleths as shown in the bottom line in Fig. 3.11 calculated for water undersaturation. b) Pseudosection and molar isopleths calculated for the depleted bulk rock composition after the first garnet growth stage (see Fig. 3.11); the rectangle marks the enlargement shown in c). d) Pseudosection and molar isopleths calculated for the bulk rock composition after the second garnet growth stage, the rectangle marks the enlargement in e). Due to the enhanced garnet growth caused by limited water in the system, fractionation effects are strong causing interrupted garnet growth also in case of water undersaturation of the host rock.

It is remarkable that also in case of water undersaturation of the host rock, which causes higher modal amounts of garnet than under water saturated conditions, fractional crystallisation leads to growth interruptions during the metamorphic evolution. The pseudosections shown in Fig. 3.12 demonstrate the P-T-X evolution of this sample assuming water undersaturation. Fig. 3.12a, which is the same diagram as the lowermost pseudosection in Fig. 3.11, displays the phase relations in the undepleted bulk rock composition. Garnet is stable in the entire grid and has high modal abundances even at greenschist-facies conditions. Due to the high amount of garnet, fractional crystallisation has a pronounced effect on the effective bulk rock composition. After a short period of garnet growth, depletion of the bulk rock composition leads to a rapid decrease in garnet abundance in the entire grid (Fig. 3.12b). The diagram in Fig. 3.12c shows the enlarged P-T area marked by the rectangle in Fig. 3.12b and demonstrates how isothermal compression of the sample leads into a phase field where garnet is not part of the stable mineral assemblage. If no or only few garnet material is recycled into the effective bulk rock composition, garnet growth will be interrupted during compression between 0.8 and 0.9 GPa. The P-T-X relations after the second garnet growth stage are displayed in Fig. 3.12d and e. Due to the strongly curved zero mode line of garnet, the rock leaves the garnet stability field at around 1.1 GPa and the stable assemblage then consists of feldspar, sodic amphibole, omphacite, phengite, epidote and quartz (Fig. 3.12e).

3.4.3.7 MK 117 (group III)

As mentioned above garnets in this sample clearly show a bimodal distribution, such that group III garnets have generally smaller grain sizes (0.1-0.5 mm) than group II garnets (1-5 mm). Thus the question arises, whether group III garnets in this sample grew during the second and third growth stage predicted by the thermodynamic forward model (Fig. 3.12). Although the growth interruptions predicted by the forward model only occur over a small P-T range (Fig. 3.12c and e) it might be the case that resorption affected at least parts of the fractionated garnet grains during the growth interruption. In order to test this possibility we modelled garnet growth in this sample starting at 0.8 GPa assuming that garnets grown during the first growth stage are completely resorbed.

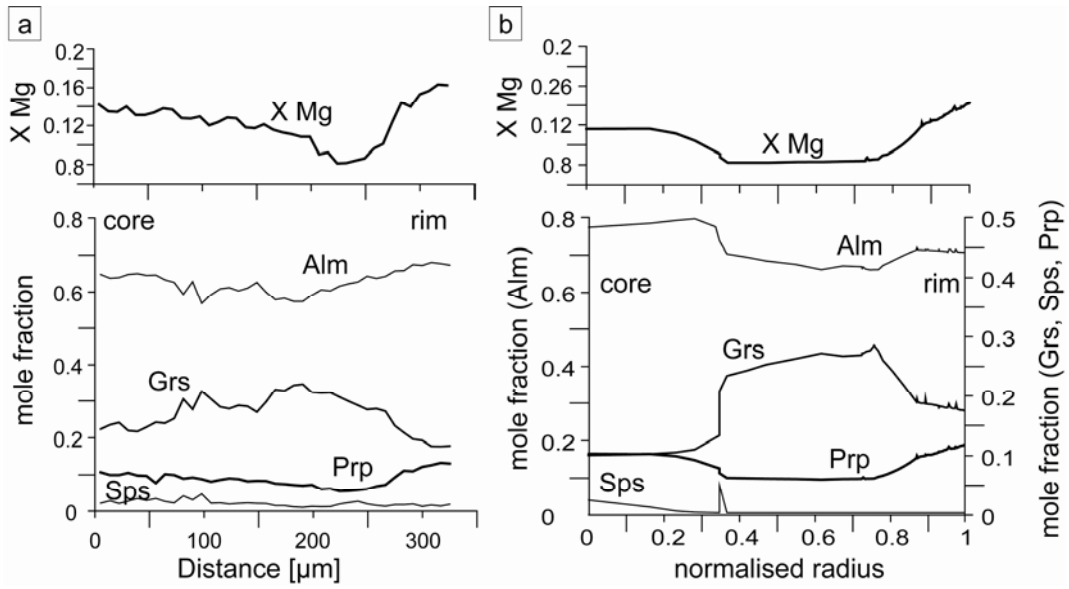

Fig. 3.13: a) Compositional core-to-rim profile across the group III garnet shown in Fig. 3.4c. b) Calculated compositional profile modelled for garnet growth along path 3, but starting at 400°C and 0.8 GPa. The profile is calculated assuming water undersaturation of the host rock and complete garnet resorption after the first growth stage.

Fig. 3.13 shows a comparison between the core-to-rim profile across the garnet shown in Fig. 3.4c (Fig. 3.13a) and the zonation pattern modelled along path 3 but starting with an undepleted bulk rock composition at 0.8 GPa (Fig. 3.13b). Although the absolute values of the garnet components are slightly different, especially in the core, the relative changes in the modelled profile resemble closely that from the natural sample. Both, almandine and pyrope show a small plateau in the core followed by a slight decrease towards the inner rim and increasing values to the outer rim. Grossular shows, as in the natural sample, the opposite trend. Although the slight increase in spessartine, the result of decreasing garnet growth, is further towards the rim in the natural profile, a stage with reduced garnet production is predicted by the model. It is therefore very likely, that garnet growth in this sample occurred in at least three stages. Whereas group II garnets record all stages of garnet growth, group III garnets grew later in the metamorphic evolution and do not record the initial garnet growth stage in this sample. The fact that both, group II and group III garnet occur in this sample might be due to small scale chemical domains leading to different effective bulk rock compositions within the sample.

3.4.3.8 MK 163 (group III garnets)

Fig. 3.14 shows the modelled zonation patterns for sample MK 163 assuming water-saturated conditions along the three different high-pressure paths. The zonation patterns are similar to those calculated for the other samples along the same paths. Almandine and pyrope contents are steadily increasing from core to rim, grossular and spessartine are steadily decreasing.

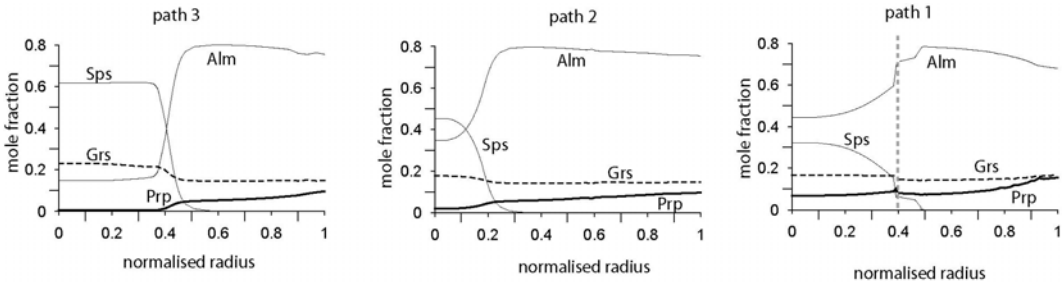

Fig. 3.14: Modelled garnet zonation patterns for sample MK 163 (group III garnets) and dehydration during metamorphism. The growth zonation patterns are similar to those obtained from other calculations assuming dehydration during the prograde evolution. The typical bell-shaped Spessartine-pattern as well as the drastically increasing Almandine content contrasts with the observed zonation pattern in the sample.

The complex zonation pattern observed in the natural sample (Fig. 3.5b) cannot be reproduced in these calculations. The zonation pattern and the amount of garnet produced at every step (growth increment) calculated for this sample assuming water-undersaturated conditions along path 3 are shown in Fig. 3.15a and b respectively. As in the calculations assuming water-saturated conditions (Fig. 3.14) the modelled zonation patterns does not show the same features as the pattern from the natural sample (Fig.3.5b). Neither the high spessartine and low almandine content in the core, nor the plateau-like pattern of grossular can be observed in the measured profile from sample MK 163. The calculated garnet growth increment shows a narrow peak after initial garnet growth (Fig. 3.15b) followed by a large period of interrupted garnet growth. This zone of hindered garnet growth might enable garnet resorption in natural rocks during prograde metamorphism. Therefore, as in the previous sample, we calculated garnet growth under water-undersaturated conditions along path 3 but assuming complete garnet resorption after the initial garnet growth period. Fig. 3.15c shows the modelled garnet zonation pattern calculated for garnet growth starting at 400°C at 0.85 GPa, which coincides with the growth interruption shown in Fig. 3.15b. Although the absolute values of the main components differ between modelled and measured zonation pattern, the relative compositional changes in the calculated pattern

resemble those observed in the natural sample (Fig. 3.15d). In both cases almandine increases slightly to the transition between inner and outer rim, followed by a decrease towards the core-rim transition. Grossular shows the opposite pattern up to this point. At the inner rim, almandine and grossular become parallel and both show a slightly decreasing plateau towards the outer rim.

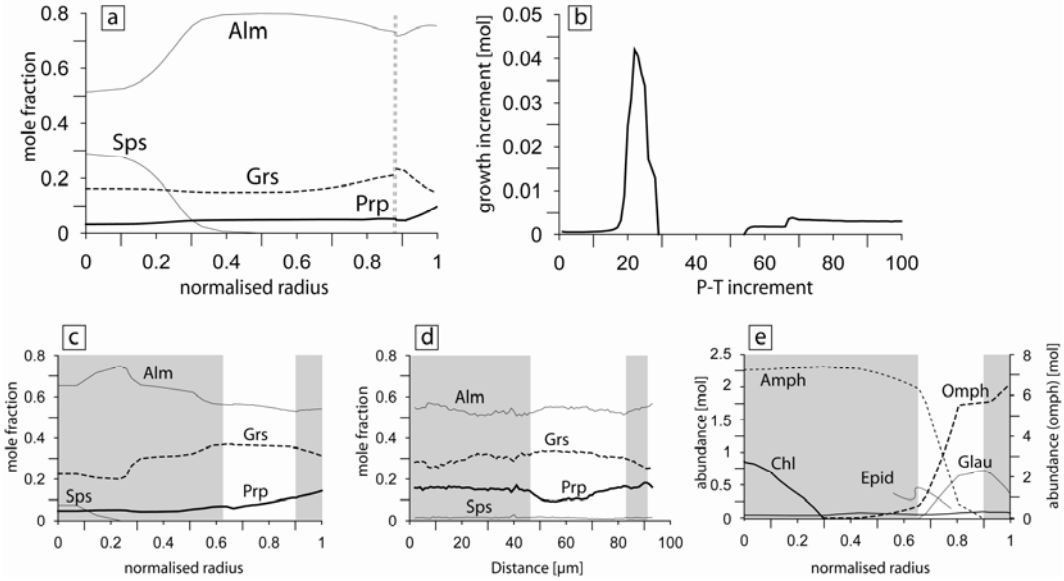

Fig. 3.15: a) Modelled growth zonation pattern for the same sample as in Fig. 3.11 but with water undersaturation of the host rock. b) Calculated amount of garnet produced at every P-T increment. Garnet growth occurs in two distinct phases separated by a large gap that marks a growth interruption during the prograde metamorphic evolution; c) and e) Calculated growth zonation pattern and mineral abundances assuming garnet resorption during the growth interruption shown in b). Initial garnet growth occurs in the presence of calcic amphibole and is mainly at the expense of chlorite, resulting in a distinct zonation pattern with opposite trends in almandine and grossular contents (left grey shaded area). The consumption of calcic amphibole causes a parallel compositional evolution of almandine and grossular (white area). d) The same almandine and grossular evolution can be observed in the natural sample.

At the outer rim, almandine and grossular again show the opposite trend. The pyrope pattern shows the characteristic decrease at the core-rim transition followed by a steady increase towards the rim. Fig. 3.15e shows the modelled mineral abundances plotted for the calculated garnet grain radius for these calculations. This clearly shows the correlation between the mineral paragenesis and the garnet growth zonation pattern. At initial growth garnet consumes mainly chlorite and coexists with calcic amphibole and epidote. In this growth period almandine and grossular show an opposite compositional trend. At the core-rim transition, at about 60% maximum radius, calcic amphibole is consumed and the

abundances of omphacite and sodic amphibole are rapidly increasing. This is the growth stage, where almandine and grossular show a parallel compositional trend and pyrope shows the characteristic decrease in its pattern. The composition of the outermost rim is influenced by the breakdown of sodic amphibole, which causes an opposite trend in almandine and grossular components. These results, together with the observation that no group II garnets occur in this sample, indicate that resorption after initial garnet growth was more intense in this sample than in MK 117, resulting in a complete recycling of the garnet material into the reacting bulk rock composition.

3.5 DISCUSSION

3.5.1 P-T path information

The modelled garnet zonation patterns differ significantly for the three modelled P-T trajectories as well as for different water contents of the protolith. Thus, interpreting the shape of the P-T path in rocks with suspected water influx is not straightforward. For example, the pattern for group I garnets in sample MK 35 modelled by assuming water-saturated conditions along path 2 (Fig. 3.7a) is similar to the pattern modelled for dehydration-only along path 3 (Fig. 3.7b). In both cases, pyrope and XMg rise steadily, except for a slight decrease along a small segment after the compositional break. This feature is also observed in the natural sample (Fig. 3.3c). In contrast to the pattern calculated for dehydration-only, the pattern in the water-saturated models additionally shows a rise in grossular content and a slight decrease in pyrope content prior to the compositional break. We take this as evidence that these model conditions are similar to those during garnet growth in the natural sample. This implies that rocks containing group I garnets followed a pressure-sensitive, rather than a temperature-sensitive P-T-path under water-saturated or nearly water-saturated conditions. Although there is very little information about the prograde evolution of the Sesia rocks, the assumption of a fast, high dP/dT subduction path with sufficient water supply is consistent with several publications reporting prograde and also retrograde lawsonite in rocks from the southern part of the Mombarone Unit (Compagnoni, 1977; Pognante, 1989). The importance of constraining the P-T-path is demonstrated in Fig. 3.16. This plot shows the calculated densities of the rocks and the water content in hydrous minerals for P-T paths 1 and 3 assuming

continuous dehydration. Also shown is the rock's water content calculated for the water-saturated model along path 3 and the amounts of garnet and omphacite calculated for the dehydration model.

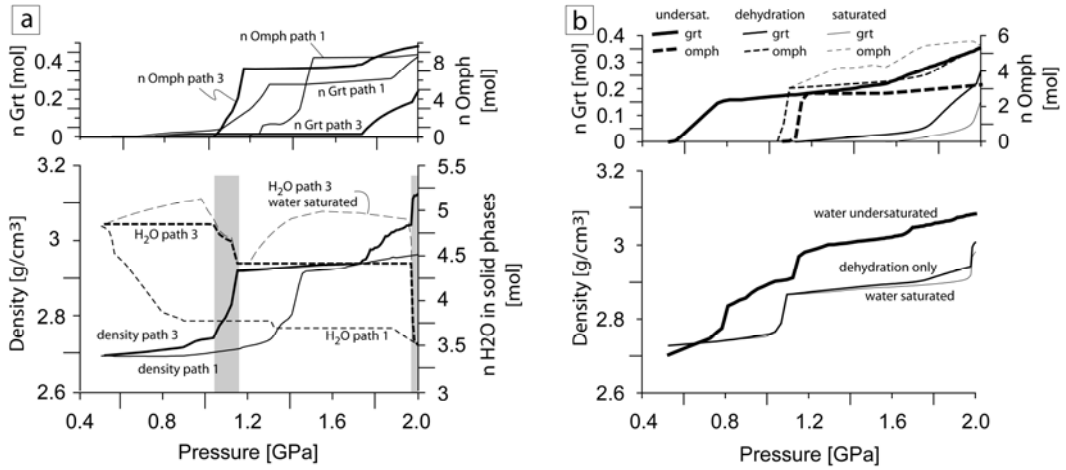

Fig. 3.16: The influence of water content and P-T paths on the physical properties of the subducted slab. a) Molar garnet and omphacite abundance, densities and water content of the subducted rocks for contrasting P-T paths (paths 1 and 3). Different omphacite and garnet evolution leads to a density contrast for the two P-T paths between 1.0 to 1.5 GPa and 1.7 to 2.0 GPa. For path 3, intense dehydration and density changes occur within small P-T intervals (shaded areas). For path 1, dehydration and density changes occur only at the transition to eclogite facies. The thin stippled line (H_2O in water-saturated rocks) shows that water-saturated rocks need intense re-hydration between 1.2 and 1.6 GPa. b) Molar abundance of omphacite and garnet and density evolution with respect to the rock's water content. See text for discussion.

These plots clearly show that the densities differ significantly for pressures between 1.0 and 1.5 GPa, such that rocks following a pressure-sensitive path are much denser at the same depths than rocks following a more temperature-sensitive path. This is mainly due to the transformation of plagioclase to omphacite, shown in the upper plot of Fig. 3.16a. The density difference is absent between 1.5 and 1.8 GPa. Interestingly, rocks following path 3 show a significant increase in density between 1.7 and 2.0 GPa, which is caused by intense garnet crystallisation above 1.7 GPa. The amount of water liberated by dehydration reactions affects the style of the subduction zone through its influence on the fluid-induced melt production (e.g. Schmid and Poli, 1998) and the rheologic behaviour of the rocks. Fig. 3.16a shows that the amount of water liberated from the subducted slab differs significantly for the different P-T trajectories. Whereas rocks along path 1 undergo intense dehydration between 0.5 and 0.9 GPa, the main water-producing reaction in rocks following path 3 occur between 1.0 and 1.3 GPa. At the transition to eclogite facies (above 1.8 GPa), all of the rocks

undergo intense dehydration. Furthermore, for path 3, the dehydration of the subducted rocks and the main density changes due to phase transformations occur within the same narrow pressure range between 1.0 and 1.2 GPa. The coincidence of dehydration reactions with density changes is expected to have a significant influence on the rheological behaviour of the subducted slab; it may facilitate earthquake generation by locally augmenting pore fluid pressure (e.g. Wintsch et al., 1995) and may water-induced weakening may possibly facilitate slab breakoff.

Fig. 3.16a shows another important property of subducted rocks: water-saturated conditions in subducted rocks need intense water influx to maintain water saturation between 1.2 and 1.8 GPa. The curve labelled "H_2O path 3 water saturated" clearly shows, that rocks following path 3 are water-undersaturated between 0.5 and 1.0 GPa and between 1.2 and 1.9 GPa. This in an important observation, because it indicates that water-saturated conditions in HP rocks can only be achieved by intense re-hydration and water-addition during burial, a crucial implication for thermodynamic equilibrium calculations.

3.5.2 Water under-saturation

The evolution of the fluid phase during subduction is a heavily discussed topic of multiple interest (Kerrick and Connolly, 1998; Schmidt and Poli, 1998; Kerrick and Connolly, 2001), because the fluids released by devolatilisation reactions may cause subduction-related volcanism, are responsible for intermediate depth earthquakes (e.g. Wiens, 2001; Tibi et al., 2003; Bock et al., 2000; Jung et al., 2004; Mishra and Zhao, 2004; Zhang et al., 2004) or can be recycled into the exosphere through the upper plate, which significantly contributes to the earth's fluid cycle. Additionally the water content of the subducted slab influences the mineral parageneses and therefore partly controls the physical properties of the subducted material.

Our models assuming initial water-undersaturation of the subducted rocks show that garnet composition at lower P-T conditions is significantly different than in water-saturated rocks (Fig. 3.11). This results in an abrupt change in garnet composition at the transition between garnet cores and rims, a feature often observed in metamorphic garnets from different tectonic settings (e.g. O´Brien, 1997; Parkinson, 2000). Such zonation patterns are mostly interpreted to be the

result of a polymetamorphic garnet growth without absolute age constraints to deduce the tectonic evolution of the host rocks. This is because dating of spatially controlled domains of garnet porphyroblasts is no trivial task (e.g. Vance and O´Nions, 1990; Ducea et al., 2003; Thöni, 2002; Sölva et al., 2003; Thöni and Jagoutz, 1992) and often impossible in fine-grained samples. Additionally incomplete isotopic equilibration and large analytical errors caused by mineral or fluid inclusions might lead to erroneous results (e.g. Luais et al., 2001). The calculations above show that complex zonation patterns with such steep compositional gradients between core and rim composition might be the result of limited water content of the host rock prior to or during HP metamorphism. Apart from the tectonic implications, the interpretation of such chemical zonation patterns might yield insight into important mineral reactions as well as the fluid evolution in the subducted rocks.

The role of fluids during subduction has been intensively investigated using stable isotopes, such as oxygen and hydrogen (e.g. Fu et al., 2003, Nadeau et al., 1993, Yui et al., 1995, Früh-Green et al., 2001), as well as trace element distribution in (U)HP rocks (e.g. Scambelluri and Philippot, 2001). Most of the recent publications show that the amount of free fluids, present during HP-metamorphism is very limited or strongly channelized (Früh-Green, 1994) in most of the HP and UHP rocks. This can be shown by the comparison of stable isotope ratios in (U)HP fluid inclusions with the ratios observed in the unmetamorphosed protoliths (e.g. Phillipot et al., 1995, Zheng et al., 1999, Cartwright and Barnicoat, 1999) as well as by the weak equilibration of trace elements between (U)HP minerals (e.g. Scambelluri and Philippot, 2001). Fig. 3.16b shows that the density evolution of water-undersaturated rocks differs significantly from those metamorphosed with water present and those modelled for a dehydration-only scenario. Water undersaturated rocks are up to 10% denser than the hydrated equivalents at blueschist facies conditions, which is the result of enhanced fractional garnet growth under water-undersaturated conditions.

Limited fluid availability has also significant influence on the element transport mechanisms and therefore on the chemical and isotopic equilibration in the entire rock. This in turn might lead to a misinterpretation of calculated phase equilibria and absolute age constraints, which has been shown in HP metamorphic rocks from the Eastern Alps (Thöni and Jagutz, 1992). It also seems to be an

important problem in the Western Alpine Sesia Zone, as indicated by a large scatter in the isotopic age constraints of the peak metamorphism (Oberhänsli et al., 1985, Ruffet et al., 1997, Duchêne et al., 1997) and very localised re-equilibration of pre-Alpine H-T metamorphic mineral assemblages (Ridley, 1989; Stünitz, 1989).

3.5.3 Relaxation of the growth zonation due to volume diffusion

The interpretation of the garnet zonation patterns requires that the shape of the chemical zonation be mainly defined by changing garnet composition during growth. The effects of later modification due to volume diffusion have been neglected in our calculations. Volume diffusion becomes important at temperatures above 550°C. The peak metamorphic conditions for the rocks considered in this study never exceeded 600°C (Reinsch, 1979; Desmons and O´Neil, 1978; Oberhänsli et al., 1985; Koons, 1986; Vuichard and Ballévre 1988; Zuccali et al., 2002), which minimises the possibility of a significant modification of the growth zonation patterns in our samples. Because the diffusional relaxation of chemical growth zonations contains information about the duration of metamorphic events we calculated the effect of volume diffusion on a typical group II growth zonation pattern. We chose a zonation pattern with an abrupt change in composition in order to calculate the minimum time span of the metamorphic event. In Fig. 3.17a the measured Fe- and Mg-profiles across the core-rim transition in sample MK 117 is shown. Also displayed are the calculated chemical zonations assuming an initial step-like growth zonation and 550°C peak temperatures. The profiles were calculated using the diffusion data from Chakraborty and Ganguly (1992) and an effective binary diffusion coefficient among the elements Fe, Mg, Ca and Mn. The profiles that display the best-fit curves to the measured zonation pattern are calculated for duration of metamorphism of 19 Ma. This is in the range of commonly observed durations of metamorphic events. Additionally shown in Fig. 3.17b is the dependence of the calculated duration of metamorphism from the peak temperature. The calculations of the relaxation profiles shows that diffusional modification due to volume diffusion does not significantly influence the growth zonation patterns, because the intrusion depth of volume diffusion in a garnet diffusion couple is less than 50 μm, whereas the compositional changes in the measured zonation patterns is much larger (e.g. Fig. 3.2).

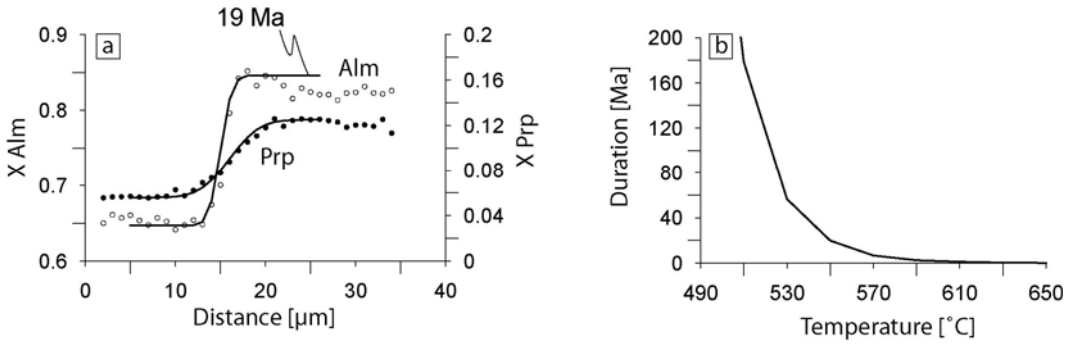

Fig. 3.17: Calculated diffusional relaxation of the step-like zonation pattern observed in sample MK 117. The curve is calculated assuming 19 Ma for the duration of HP metamorphism at peak temperatures of 550°C. b) Calculated duration of metamorphism as a function of the peak temperature for the relaxation profile in a).

In contrast to volume diffusion, a compositional modification along submicroscopic cracks seems to play a more important role in some of the samples (Fig. 3.4). Such a modification of the growth zonation is quite common in metamorphic rocks (e.g. Hames and Menard, 1993; Zack et al. 2002). In these zones element transport might be several magnitudes faster than in the undeformed garnet lattice. Therefore we have to admit that element redistribution in these zones might have an influence on the interpretation of the zonation patterns. But as these affected areas are clearly visible in the BSE image, we avoided measurements in these zones, although an influence of this modification, that seems to have much faster diffusion velocities cannot be excluded.

3.5.4 Regional implications

Past authors have debated whether all units of the Sesia Zone experienced the same evolution during Alpine HP metamorphism (Ridley, 1989; Stünitz, 1989; Spalla et al., 1991). Though knowledge of the prograde evolution is essential for investigating processes responsible for the subduction of continental lithosphere to depths greater than 50 kilometres, it is evident that the larger the coherent body of such lithosphere, the greater the magnitude of the buoyant forces that oppose subduction. In contrast, smaller slices of light continental material can be easily subducted, especially when tectonically coupled with oceanic crust. Subductibility is augmented by the density increase due to water undersaturation in large parts of the coherent lithospheric slab. Our modelling indicates that large parts of the Mombarone Unit were not fully hydrated prior to Alpine HP metamorphism. In contrast, rocks belonging to the Bonze Unit as well as in the vicinity of the nappe

contacts show evidence for water saturation prior to subduction. The three tectonic units of the Sesia Zone differ not only in lithology but also in their water-content during metamorphism. These differences in water-content in turn reflect their different P-T subduction paths and differences in their pre-Alpine (pre-HP) metamorphic evolution. Accordingly, the water-saturated rocks of the Bonze Unit and the water-undersaturated rocks of the Mombarone Unit were folded together during initial exhumation of the Mombarone Unit (cf. Ridley, 1989, Stünitz, 1989).

3.6 CONCLUSIONS

Three different types of garnet zonation patterns within the high pressure rocks of the Western Alpine Sesia Zone reflect different volatile conditions during pre-orogenic subduction and accretion of continental crust in the Western Alps. The regional correlation between garnet zonation patterns and sample locality confirms independent lithological and structural evidence, that the Sesia Zone comprises units with different metamorphic histories during subduction.

The comparison of garnet zonation patterns derived from thermodynamic forward models that consider the effects of fractional crystallisation and devolatilisation during metamorphism, with those observed in natural samples shows that these patterns are diagnostic of certain P-T paths and water content of the host rock during HP metamorphism. Group I garnets grew under water-saturated conditions or close to water saturation along a pressure-sensitive P-T path. Group II and III garnet zonation patterns reflect water-undersaturated conditions during prograde HP metamorphism. These models suggests that fluid migration was either restricted to localized channels or absent during the subduction of large segments of the Sesia Zone.

Water undersaturation during subduction has major influence on the physical properties of the subducted rocks. Due to enhanced garnet crystallisation, the density of the subducted slab increases by up to 10% with respect to their water-saturated equivalents. Further, the shape of the prograde P-T trajectory reflects the interplay between dehydration reactions and density changes within the subducted slab. In case of a “cool” (i.e. steep, pressure-sensitive) subduction path, dehydration reactions and the main density changes in the slab occur within a small P-T interval. For a warm subduction the depths of these phase transitions

do not coincide. Further our result show that the method of thermodynamic forward modelling is an excellent tool to more precisely define P-T trajectories as well as the chemical evolution of the host rock during subduction processes.

3.7 ACKNOWLEDGEMENTS

We thank Claudio Rosenberg for his comments on earlier versions of the manuscript and Christian de Capitani for his numerous helpful suggestions regarding the thermodynamic modelling. The project was funded by the German Science Foundation (DFG) grant HA 2403/5.